Journal of Experimental Botany, Vol. 70, No. 9 pp. 2479–2490, 2019
doi:10.1093/jxb/ery430 Advance Access Publication 25 February 2019
This paper is available online free of all access charges (see https://academic.oup.com/jxb/pages/openaccess for further details)

RESEARCH PAPER

A three-dimensional canopy photosynthesis model in rice with a complete description of the canopy architecture, leaf physiology, and mechanical properties

Tian-Gen Chang[1], Honglong Zhao[1,3], Ning Wang[2,3], Qing-Feng Song[1], Yi Xiao[1], Mingnan Qu[1], Xin-Guang Zhu[1,*]

[1] National Key Laboratory of Plant Molecular Genetics, CAS Center for Excellence in Molecular Plant Sciences, Shanghai Institute of Plant Physiology and Ecology, Chinese Academy of Sciences, Shanghai 200031, China
[2] CAS MPG Partner Institute for Computational Biology, Chinese Academy of Sciences, Shanghai 200031, China
[3] University of Chinese Academy of Sciences, Beijing 100049, China

* Correspondence: zhuxg@sippe.ac.cn

Received 14 May 2018; Editorial decision 3 December 2018; Accepted 8 January 2019

Editor: Pierre Martre, INRA, France

Abstract

In current rice breeding programs, morphological parameters such as plant height, leaf length and width, leaf angle, panicle architecture, and tiller number during the grain filling stage are used as major selection targets. However, so far, there is no robust approach to quantitatively define the optimal combinations of parameters that can lead to increased canopy radiation use efficiency (RUE). Here we report the development of a three-dimensional canopy photosynthesis model (3dCAP), which effectively combines three-dimensional canopy architecture, canopy vertical nitrogen distribution, a ray-tracing algorithm, and a leaf photosynthesis model. Concurrently, we developed an efficient workflow for the parameterization of 3dCAP. 3dCAP predicted daily canopy RUE for different nitrogen treatments of a given rice cultivar under different weather conditions. Using 3dCAP, we explored the influence of three canopy architectural parameters—tiller number, tiller angle and leaf angle—on canopy RUE. Under different weather conditions and different nitrogen treatments, canopy architecture optimized by manipulating these parameters can increase daily net canopy photosynthetic CO_2 uptake by 10–52%. Generally, a smaller tiller angle was predicted for most elite rice canopy architectures, especially under scattered light conditions. Results further show that similar canopy RUE can be obtained by multiple different parameter combinations; these combinations share two common features of high light absorption by leaves in the canopy and a high level of coordination between the nitrogen concentration and the light absorbed by each leaf within the canopy. Overall, this new model has potential to be used in rice ideotype design for improved canopy RUE.

Keywords: Canopy photosynthesis, 3D canopy, leaf nitrogen concentration, rice, ideotype, systems model.

Introduction

Identifying new options to increase crop yield to feed the world's population is one of most urgent tasks for agriculture in the 21st century. For cereal crops, more than 90% of the harvested dry matter is the product of photosynthesis. Improvement of canopy photosynthesis holds great potential to increase biomass and yield of cereals (Peng, 2000; Gu *et al.*,

2014; Song *et al.*, 2016*a*). Plant architecture has been recognized as the most important selection target for high canopy radiation use efficiency (RUE), and hence high yield potential (Peng, 2000), in crop breeding. Many ideotypes have been proposed for different crops in the course of breeding programs conducted over the past years. For example, Yuan (1998, 2001) proposed an ideotype for rice grown under a subtropical climate, in which the three uppermost leaves should be long, erect, narrow, V-shaped (adaxially rolled), and thick. Breeders at the International Rice Research Institute have proposed another rice ideotype, called NPT (new plant type), which has fewer tillers with dark green and erect leaves (Peng *et al.*, 1994). Chen *et al.* (2000) proposed an ideotype for *japonica* rice adapted to a temperate climate, which has erect panicles. These different ideotypes have played guiding roles in high-yield rice breeding in the past decades. However, the quantitative features of these ideotypes are empirically extracted from high-yielding lines in the breeding fields; this approach inevitably misses opportunities to identify superior combinations of features that either do not exist in current breeding populations, or exist but do not show superior performance owing to the influence of other features that have negative impacts on biomass and yield in the same line.

Crop models have been used to evaluate crop performance and identify factors limiting crop growth since the first mathematical model of crop growth was developed by de Wit (1965). To date, many crop models have been developed for different crops (see reviews by Li *et al.*, 2015; Chang and Zhu, 2017; Maiorano *et al.*, 2017). As the source of photosynthates supporting crop growth and development, canopy photosynthesis is a critical component in all these models. Models of canopy photosynthesis with different levels of mechanistic detail have been developed, which range from treating the whole canopy as 'a big leaf' (Amthor, 1994; Lloyd *et al.*, 1995) or as 'two leaves', that is, sunlit and shaded leaves (De Pury and Farquhar, 1997), to the detailed description of canopy architecture and the leaf physiological parameters of a canopy (Song *et al.*, 2013). Three-dimensional (3D) canopy photosynthesis models emerged with rapid advances in modern computing capacity; these models can directly simulate the complex 3D canopy architecture and the microclimate within the canopy. Such models have been developed for species including rice (Watanabe *et al.*, 2005; Zheng *et al.*, 2008; Xu *et al.*, 2011; Song *et al.*, 2013), maize (Fournier and Andrieu, 1998, 1999), and sugarcane (Wang *et al.*, 2017). Various ray-tracing algorithms, including a stochastic ray-tracing algorithm based on the Monte Carlo method (Tucker and Garratt, 1977; Mech, 1997), a randomized quasi-Monte Carlo sampling algorithm (Cieslak *et al.*, 2008), a reverse ray-tracing algorithm (Xu *et al.*, 2011), and a forward ray-tracing algorithm (Song *et al.*, 2013), have been developed to quantitatively predict the light environment inside a canopy. A dedicated framework, FPSM-P (functional-structural plant modelling prototype), in which the 3D canopy can be reconstructed and canopy photosynthesis can be directly calculated, has been developed recently (Henke *et al.*, 2016). There is now a strong research demand to develop methods that effectively combine accurate reconstruction of plant 3D architecture, efficient model parameterization, and on-the-fly model simulation.

Here we describe the development, parameterization, validation, and application of a new 3D rice canopy photosynthesis model (3dCAP). This model incorporates detailed and flexible 3D architecture of each organ in a rice canopy, including leaves, sheaths, stems, and panicles; an accelerated version of the forward ray-tracing model *fastTracer*; a steady-state empirical C_3 leaf photosynthesis model; and an integrated protocol of field measurement and model parameterization. Using this model, we studied the canopy characteristics of an elite *japonica* cultivar and explored the ideal plant type for this cultivar under different weather conditions and for different nitrogen treatments.

Materials and methods

Plant material, field management, and growth conditions

The field experiments were conducted at the Songjiang breeding station of the Shanghai Institutes of Plant Physiology and Ecology, Shanghai, China (31° N, 121° E). The rice (*Oryza sativa* L.) used in this study is the elite *japonica* cultivar 'Xiushui 134' (XS134). Seeds were sown on seedbeds after germination on 1 June 2015. On 26 June, seedlings were transplanted to field at a planting density of 25.0 hills m^{-2} (0.20×0.20 m per hill). Two nitrogen treatments were applied to the plants. For the high-nitrogen (HN) treatment, nitrogen fertilizer was applied at a rate of 120 kg ha^{-1} and 3:2:2 of the total nitrogen on 3 July, 21 July, and 20 August, respectively. Phosphate (P_2O_5) and potassium (K_2O) fertilizers were applied as basal fertilizers before transplantation, at 100 kg ha^{-1}. For the low-nitrogen (LN) treatment, no nitrogen was applied during the whole growth season. Weeds, pests, and diseases were controlled conventionally with periodic application of herbicides, insecticides, and fungicides. Weather data, including photosynthetically active radiation (PAR), relative humidity, and air temperature, were recorded by a WatchDog 2900ET Weather Station (Spectrum Technologies Inc., Aurora, IL, USA) every 10 minutes for the whole growth season. The rice plants started grain filling around 11 September and were harvested on 28 October. In total, 80 plots (8 lines×10 plots per line) of plants were grown for each treatment, with 49 (7×7) plants in each plot. We used a randomized block design and chose from among only the central 5×5 plants in each plot for the measurements.

Measurements of leaf and canopy level gas exchange

Leaf photosynthetic light response curves (*A*-Q curve) were measured weekly using a LI-6400 infrared analyzer (Li-Cor Inc., Lincoln, NE, USA) after 30 July 2015. To avoid effects of photosynthetic photon flux density (PPFD) fluctuation during the measurements, we designed an indoor facility (High-efficiency All-weather Photosynthetic measurements System; HAPS) and measured leaf photosynthetic parameters of plants with HAPS. A detailed description of the use of HAPS and the protocol of the *A*-Q curve measurements and data fitting can be found in Chang *et al.* (2017). Using the method described in Chang *et al.* (2017), three parameters were extracted from the *A*-Q curves: the maximum apparent quantum yield of CO_2 fixation (Φ_{CO2}), the curvature parameter (θ), and the light-saturated photosynthetic rate (A_{sat}).

Canopy-level gas exchange was measured with the Canopy Photosynthesis and Transpiration Measurement System (CAPTS), which comprises transparent chambers, sensors, and a control unit for data logging and storage. A detailed description of the design and performance of CAPTS and the protocol used for data acquisition and analysis are provided in Song *et al.* (2016*b*).

Measurements and extraction of parameters for 3D rice architecture reconstruction

To obtain the parameters used for 3D canopy reconstruction, we measured parameters in five plants from five randomly chosen plots. First, we took photographs of the standing plants with a digital camera (DSLR D7100, Nikon, Tokyo, Japan), and then the tiller number of each plant was counted. Second, the tillers of each plant were detached, and photographs of the biggest, the middle, and the smallest tillers of each plant were taken. Third, leaves on each of these tillers were detached and photographs were taken to determine the two-dimensional (2D) morphology of these leaves. At the same time, leaf sheaths were detached and photographs of the sheaths, stem, and panicle were taken. Fourth, to quantify the panicle branching pattern, the panicle was spread and scanned with an Epson Perfection V300 Photo scanner (Epson, Tokyo, Japan). Finally, the grains on each panicle were threshed from the panicle and photographed.

Five MATLAB (The MathWorks Inc., Natick, MA, USA) scripts were developed to automatically extract features from digital photographs of the tillers, leaves and sheaths, internodes, panicle, and grains. These features were the tiller number, internode length and thickness, leaf sheath length, leaf basal angle to the stem, leaf curvature, leaf length, leaf width, panicle length, length and thickness of primary branches and their distribution pattern on the rachis, grain number, grain length, and grain width. The compiled scripts are available at https://rootchang.github.io/3dCAP/.

Reconstruction of canopy architecture

Modelling the 3D structure of the different organs and assembly of these organs into a plant and canopy are described below. Plant organs in the canopy were triangulated and stored as small indexed facets.

Reconstruction of a leaf

Following Watanabe *et al.* (2005), the patterns of leaf width change from leaf base to tip were classified into two groups, that is, the pattern of leaf width change in the flag leaf and the pattern of leaf width change in other leaves. In each group, the changes in leaf width along the leaf length was modelled with a piecewise cubic Hermite polynomial (Fritsch and Carlson, 1980) based on the widths (normalized to 0–1) at seven points along the leaf length and the maximal width of the leaf (see Supplementary Fig. S1A, B at *JXB* online). The curvature of a leaf was modelled with an ever-increasing leaf angle along the horizontal direction as follows:

$$\Delta\alpha_x = k_0 \cdot x^n \tag{1}$$

$$\alpha_x = \alpha_0 + \int_0^x \Delta\alpha_y dy \tag{2}$$

where k_0 is a fitted coefficient, x is a projected leaf length in the horizontal direction, α_0 is leaf basal angle to the vertical direction, and n is the polynomial order, which can be either 1 or 2 in the model. When α_0 and the coordinates of the leaf base (x_0, y_0) are given, k_0 was iteratively solved by fitting the coordinates of the leaf tip (x_1, y_1) (Supplementary Fig. S1C, E). The adaxial rolling of a leaf was defined based on the start position of rolling (x_{r0}) on the leaf and the rolling radius of the cross-section (R_r; Supplementary Fig. S1D); the adaxial twisting of a leaf was modelled with three parameters, the start position twisting (x_{t0}) on the leaf, the total twisting angle (α_t), and the terminal position of twisting (x_{t1}; Supplementary Fig. S1F).

Reconstruction of an internode and a sheath

Both the internode and sheath were simplified as cylinders. As a result, four parameters were needed for reconstruction of an internode or sheath: the position (x_0, y_0) and radius (R_0) of the base circle and the position (x_1, y_1) and radius (R_1) of the tip circle of the cylinder.

Reconstruction of a panicle

The rice panicle has a complex branching structure. For simplification, only the primary branches were considered. First, the 2D structure was reconstructed based on the grain number and size, the thickness of the rachis, primary branches, and spikelet branches along their length, the total primary branch number, the positions and initial angles of branches attaching on the rachis, the length of the branches and rachis, the relative position of the first grain on a branch, and the average distance between grains on the branches. Specifically, the rachis and branches were modelled as quadrangle prisms, and grains were modelled as two back-to-back quadrangle prisms (Fig. 1A).

The 3D architecture of a panicle was modelled with a mechanical model. First, the rachis was divided into small segments. The bending angle of each segment on the rachis was approximated by treating each primary branch as a free-hanging mass point on an elastic rod (Fig. 1B):

$$\Delta\theta_i = \frac{\sum_{j=i}^{N} 2 \cdot F_j \cdot \theta_i \cdot s_i \cdot (2 \cdot L_j - s_i)}{Y \cdot \pi \cdot r_i^4} \tag{3}$$

where θ_i is the initial angle of the ith segment, F_j is the force of gravity generated by the jth branch, s_i is the length of the ith segment, r_i is the radius of the ith segment, L_j is the equivalent length of the base of the jth branch to the ith segment, and Y is the Young's modulus of the rachis and branches, which is estimated empirically. Initially, all the θ_i were set to θ_0, which was the basal angle of the panicle. Then, each θ_i was sequentially updated iteratively based on the above equation until all θ_i were stabilized. After the posture of the rachis was set, the curvature of each primary branch was determined similarly by treating each grain on the branch as a free-hanging mass point on an elastic rod.

The 3D panicle architecture was simulated based on the current total grain weight and grain weight distribution on each branch. For example, the dynamic 3D panicle architecture during the grain filling period of a typical *indica* rice cultivar was simulated (Fig. 1C), and the final architecture at harvest was close to that observed (Fig. 1D).

Reconstruction of a tiller, a plant, and a canopy

An intact tiller can be reconstructed by assembling the reconstructed individual organs described above. As a simplification, the average value of each feature used in the reconstruction of organs was used to construct tillers in a plant, with each value multiplied by a Gaussian random disturbance $N(1,\sigma)$ where the standard error σ determines the uniformity of tillers. The bases of tillers in a plant were modelled to be located on concentric circles. The tiller number on each circle was assumed to form a triangular number sequence (i.e. 1, 3, 6, 10, etc.). The tiller angle of tillers on the ith circle was modelled as:

$$\alpha_i = \frac{\alpha_0 \cdot i}{2} \tag{4}$$

where α_0 is the estimated tiller angle constant. The tillers on each circle are randomly orientated. Finally, a canopy with 3×3 plants can be generated by the reconstruction of 9 plants independently.

Simulation of canopy light distribution

After reconstruction of a canopy, a previously developed forward ray-tracing algorithm, *fastTracer*, was applied to simulate light distribution within the canopy (Song *et al.*, 2013). Leaf optical properties were modelled based on chlorophyll content by fitting the PROSPECT-5 model (Feret *et al.*, 2008):

$$K_r = 0.3605 \cdot [\text{chl}]^{(-0.502)} \tag{5}$$

$$K_t = -0.082 \cdot \log([\text{chl}]) + 0.3761 \tag{6}$$

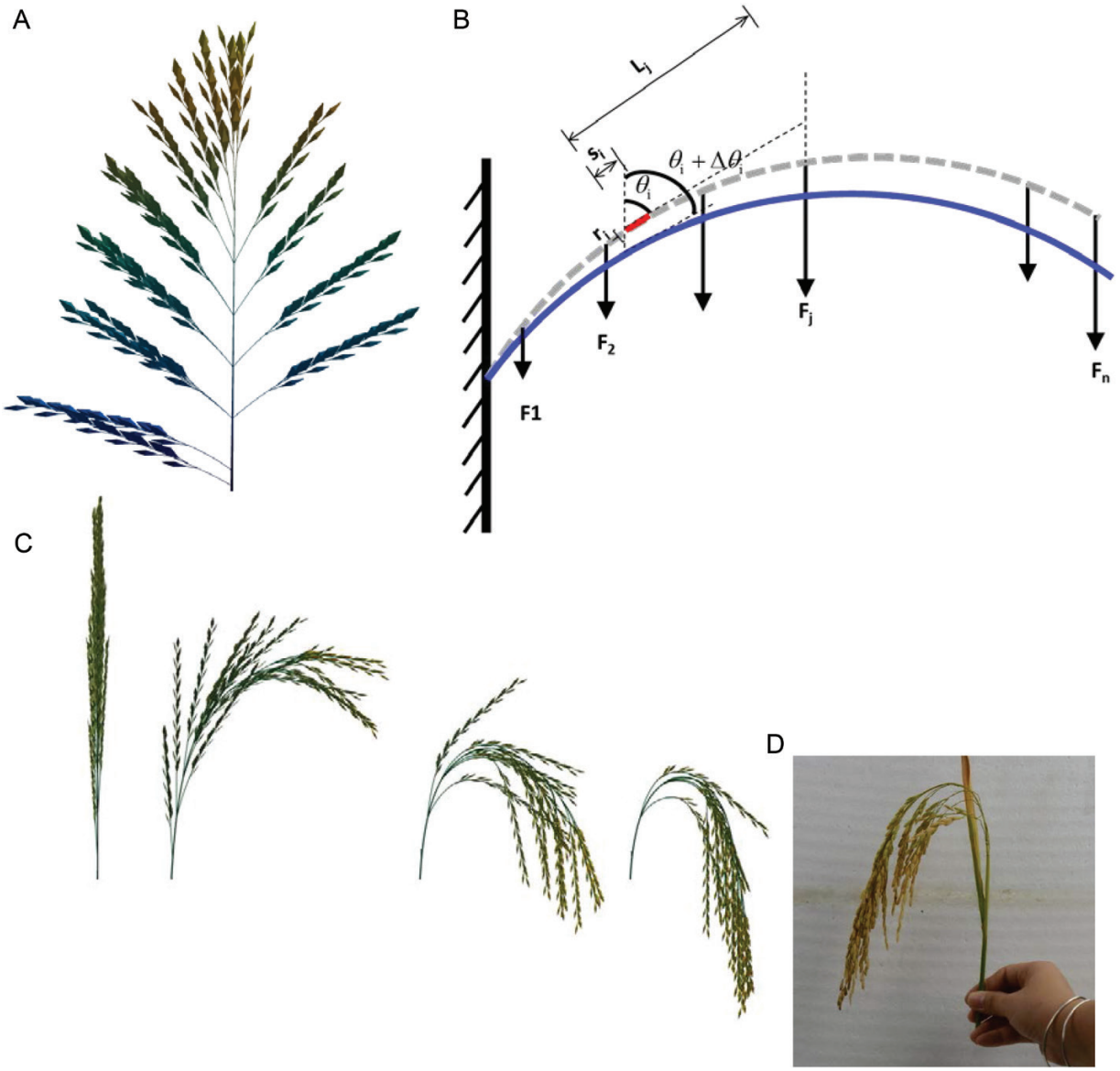

Fig. 1. Reconstruction of the 2D and 3D architecture of a rice panicle. (A) The simulated 2D architecture of a rice panicle. (B) An illustration of the mechanical model used to simulate the bending of the rachis or one of the primary branches. θ_i, Initial angle of the *i*th segment; $\Delta\theta_i$, bending angle of the *i*th segment; F_j, force of gravity generated by the *j*th branch; s_i, length of the *i*th segment; r_i, radius of the *i*th segment; L_j, equivalent length of the base of the *j*th branch to the *i*th segment; *Y*, Young's modulus of the rachis and branches. (C) Simulated changes of the 3D architecture of a panicle for an *indica* rice cultivar during the grain filling period. (D) Photograph of a real panicle at harvest.

where K_r and K_t are the reflected and transmitted proportion of total incident light on the leaf, respectively, and [chl] is the leaf chlorophyll content (μg cm^{-2}). We converted leaf nitrogen concentration to leaf chlorophyll content by numerically integrating empirical equations developed by Peng *et al.* (1993) and Markwell *et al.* (1995):

$$\mathrm{SLN} = \mathrm{SLW} \cdot \mathrm{LNC}/100 \tag{7}$$

$$[\mathrm{chl}] = 7.252 \cdot \mathrm{SLN}^2 + 18.191 \cdot \mathrm{SLN} + 1.5012 \tag{8}$$

where SLN is the specific leaf nitrogen content (g N m^{-2}), SLW is the specific leaf weight (g m^{-2}) and LNC is the leaf nitrogen concentration (% or g g^{-1}). K_t of grains and sheaths were set to 0.

To speed up the computation, direct and scattered light were simulated separately using *fastTracer*. The light distribution inside a canopy was predicted for four time points of a day: 06.00, 08.00, 10.00, and 12.00 h. Canopy light distribution patterns at 14.00, 16.00, and 18.00 h were assumed to be the same as those at 10.00, 08.00 and 06.00 h, respectively. The scattered light distribution pattern in the canopy was simulated only once for one day. Then, the total light absorbed by the different organs in a canopy was calculated based on the direct/scattered light distribution patterns and the direct/scattered incident PPFD above the canopy at that time.

Calculation of canopy photosynthesis

The net photosynthetic rate of a facet *j* on leaf *i* at time *t* ($A_{n\_ij,t}$) was calculated using the non-rectangular hyperbola model:

$$A_{n\_ij,t} = \frac{\Phi_{CO2}(i) \cdot I(ij,t) + A_{sat}(i) - \sqrt{(\Phi_{CO2}(i) \cdot I(ij,t) + A_{sat}(i))^2 - 4 \cdot \Phi_{CO2}(i) \cdot \theta(i) \cdot I(ij,t) \cdot A_{sat}(i)}}{2\theta(i)} - R_d(i) \tag{9}$$

where I is the incident light intensity, Φ_{CO2} is the apparent quantum yield, θ is the empirical curvature coefficient, A_{sat} is the light saturated gross

photosynthetic rate, and R_d is the dark respiration rate (assumed to be 0.5 μmol m^{-2} s^{-1}). The photosynthetic parameters were fitted based on the LNC of the ith leaf (LNC_i):

$$\Phi_{CO2}(i) = a_0 \cdot LNC_i^2 + a_1 \cdot LNC_i + a_2 \quad (10)$$

$$A_{sat}(i) = b_0 \cdot LNC_i^2 + b_1 \cdot LNC_i + b_2 \quad (11)$$

$$\theta(i) = c_0 \cdot LNC_i^2 + c_1 \cdot LNC_i + c_2 \quad (12)$$

where a_0, a_1, a_2, b_0, b_1, b_2, c_0, c_1, c_2 are the fitting coefficients.

The average net photosynthetic rate of the ith leaf of a tiller at time t ($A_{n\_i,t}$) can be calculated as:

$$A_{n\_i,t} = \frac{1}{m_i} \sum_{j=1}^{m_i} A_{n\_ij,t} \quad (13)$$

where m_i is the total number of facets on leaf i.

The net canopy photosynthetic rate at time t ($A_{c,t}$) was calculated by adding the net photosynthesis of all the leaves in a canopy:

$$A_{c,t} = TN \cdot \sum_{i=1}^{m} LA_i \cdot A_{n\_i,t} \quad (14)$$

where TN is the total tiller number per land area, LA_i is area of the ith leaf on a tiller, and m is the total number of leaves on a tiller.

The daily net canopy photosynthetic accumulation (ACP) was calculated by integrating $A_{c,t}$:

$$ACP = \int_{t=6}^{18} A_{c,t}\, dt \quad (15)$$

Results

Construction and parameterization of a 3D canopy photosynthesis model

The new integrated model, 3dCAP, comprises three sub-models: the canopy architecture model, the ray-tracing model, and the leaf photosynthesis and respiration model. The workflow of 3dCAP is illustrated in Supplementary Fig. S2. First, the 2D and 3D structure of individual organs (i.e. the leaf, sheath, stem, and panicle) were reconstructed. These organs were assembled into a rice tiller. Then, different tillers were arranged to form a rice plant. A canopy was then generated by arranging plants with a certain distance between them in both the row and column directions. A forward ray-tracing algorithm was applied to simulate canopy light distribution with a given canopy vertical nitrogen distribution, incident light, and canopy architecture. Finally, the canopy gas exchange rate was calculated by summing gas exchange rates for individual leaves, which were calculated by a semi-empirical C_3 photosynthesis light response model.

Fig. 2 illustrates the workflow for extraction of parameters from photographs. First, photographs of standing rice plants were taken. Then, the tillers were detached from the plants and photographed. Five parameters were extracted for each leaf on the tiller: the leaf base height (P1), leaf length (P2), leaf base angle (P3), leaf vertical length (P4), and leaf horizontal length (P5). Leaves were then detached to extract additional 2D features: the leaf width at seven different positions along the length of the leaf (P6–P12), the maximal leaf width (P14), and the leaf length (P13). Next, leaf sheaths were detached and the length of each one (P15) was extracted. The length of the panicle (P16) and the length (P17) and diameter (P18) of each internode were then extracted. After this, the panicle was scanned digitally to extract detailed 2D features: the diameter of the rachis (P19) and the base height (P20), length (P21), and diameter (P22) of each primary branch. Finally, the grains were threshed off the panicle and photographed, and the grain number (P23), grain length (P24), and grain width (P25) were quantified from the photographs. The average values and variations of these parameters are listed in Table 1.

Leaf photosynthetic properties were calculated based on a derived relationship between LNC and leaf photosynthetic parameters (equations 13–15). As a result, A_{sat} and Φ_{CO2} had a quadratic relationship with LNC for both HN- and LN-treated plants, whereas θ was unrelated to LNC (Fig. 3), which in this study was set to the average of measured values, that is, 0.512 for HN-treated and 0.587 for LN-treated plants.

Reconstruction of the 3D plant architecture and prediction of canopy-level gas exchange under different weather conditions and nitrogen treatments

After extracting plant architectural parameters from the digital photographs, the 3D plant architecture can be reconstructed (Supplementary Fig. S3). A visual comparison showed that the reconstructed plants mimicked the real plants in both the HN and LN treatments (Fig. 4A, B, E, F). We further compared the horizontal and vertical distribution of the number of 'plant pixels', that is, pixels representing plant tissue in the images. Results showed consistency between the reconstructed and real plants (Fig. 4C, D, G, H), although there were larger differences for the distribution of vertical 'plant pixels' at the bottom of plants owing to the presence of some senescent leaves and sheaths in the images of real plants, which were not considered during the 3D reconstruction (Fig. 4D, H).

We compared the modelled and measured canopy photosynthetic rates. First, modelled and measured values for net canopy photosynthesis during the daytime were compared. Simulations for three typical weather conditions—a sunny, a cloudy, and an overcast day— were used for the comparison (Fig. 5A–C). Results showed that 3dCAP accurately predicted the daily dynamic canopy photosynthesis on the overcast and cloudy days (Fig. 5D, E, G, H), but underestimated canopy photosynthesis slightly on the sunny day in the morning and under high light at noon (Fig. 5F, I). This result might be due to a higher leaf photosynthetic rate in the morning than at noon and in the afternoon on a sunny day (Ishihara and Saitoh, 1987). In addition, some other photosynthetically active organs, such as panicles and leaf sheaths, might contribute to canopy photosynthesis under high light, and this possibility is not considered in the current model.

We further collected all the measured canopy photosynthesis data from 11 to 18 September. We categorized these data into three groups based on the time of day: early morning and late afternoon (06.00 to 08.00 h and 16.00 to 18.00 h;

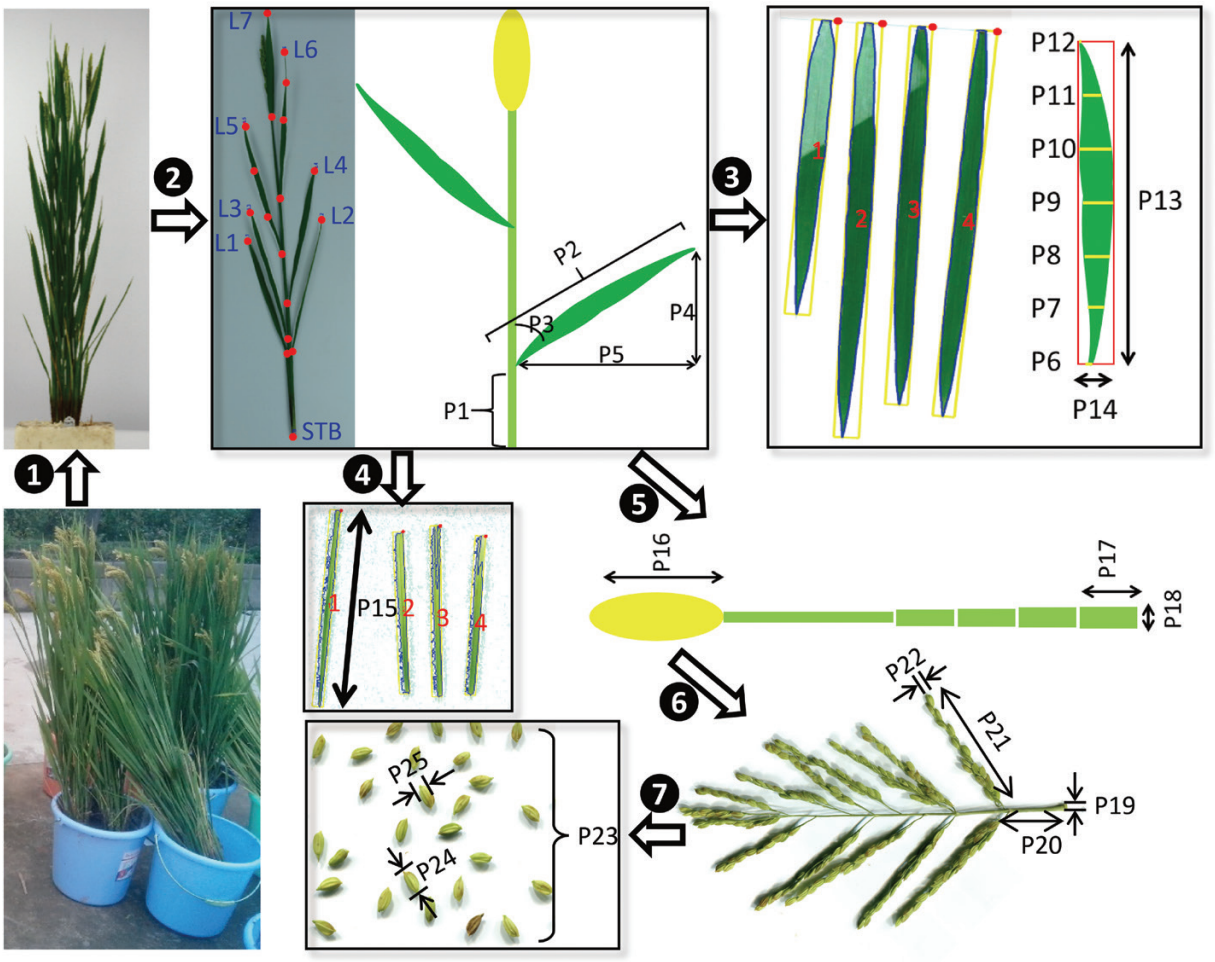

Fig. 2. Illustration of the workflow for canopy architecture measurement using rice directly taken from the field. The architectural parameters used in the 3D model construction are labelled P1 to P25.

Supplementary Fig. S4A, D), mid-morning and mid-afternoon (08.00 to 10.00 h and 14.00 to 16.00 h; Supplementary Fig. S4C, F), and noontime (10.00 to 12.00 h and 12.00 to 14.00 h; Supplementary Fig. S4B, E). We simulated canopy photosynthetic CO_2 uptake rate in these three periods, assuming all incident light was either direct light or scattered light. Simulated results were in line with the measured data (Supplementary Fig. S4). The simulation also showed that canopy photosynthesis under direct light was lower than that under scattered light in the morning and the late afternoon, especially under high light levels (Supplementary Fig. S4A) and also under the HN treatment, for which the canopy had a higher leaf area index (Supplementary Fig. S4D). However, at noontime, the canopy photosynthetic rate was predicted to be higher under direct light than scattered light (Supplementary Fig. S4C, F), especially when the leaf area index was high (Supplementary Fig. S4F).

Optimizing canopy photosynthetic CO_2 uptake rate under different weather conditions

We further explored canopy architectures that can lead to higher ACP for plants grown in both LN and HN conditions. We enumerated all possible canopy architectures with tiller number, tiller angle, and leaf angle ranging from 5 to 20-fold (step size=1), 0.2 to 2-fold (of default values, step size=0.2), and 0.2 to 2.6-fold (of default values, step size=0.2), respectively. In total, we predicted ACP for 2080 plant architectures for each nitrogen treatment. The ACP for each of these architectures under four different light environments—strong direct light (Fig. 6A), strong scattered light (Fig. 6F), weak direct light (Fig. 6K), and weak scattered light (Fig. 6P)—were simulated and ranked. We found that the ACP of the top 50 architectures was 16–20% and 10–52% higher than that of the default canopy under the LN and HN treatments, respectively (Fig. 6B, G, L, Q). However, the canopy architectural parameters (i.e. tiller number, tiller angle, and leaf angle) in the top 50 architectures all varied greatly between different light conditions and different nitrogen treatments (Fig. 6C–E, H–J, M–O, R–T). Even under the same light and nitrogen conditions, these parameters, in particular tiller angle, showed great variation among the top 50 architectures (e.g. Fig. 6C–E). To further illustrate this point, for each light environment and nitrogen treatment, we identified two dramatically different plant architectures taken from the top 50 plant architectures that had similarly high ACP (Supplementary Fig. S5). These results indicate that the maximal ACP is the result of a coordination between canopy architectural features. In other words, the optimal value for

Table 1. *Major parameters and their values collected for rice cultivar XS134 grown under high-nitrogen or low-nitrogen treatment* (n≥5).

NT	LP	LL	LW	LA	LBA	LNC	SLW	LSL	IL	TN	PL	PBN	TGN
HN	1	22.5±4	1.57±0.43	25.4±10.7	0.04±0.02	3.15±0.58	51.6±8.8	19.4±7.1	24.5±4.6	11.7±3.0	17.4±0.2	14.9±2.7	210±22
	2	26.2±8.9	1.46±0.42	31.2±16.1	0.13±0.11	3.06±0.47	47.6±9.9	18.2±3.5	15.9±0.8				
	3	33.2±2.2	1.62±0.15	41.1±4.8	0.17±0.06	3.09±0.11	52.4±6.8	20.9±1.2	12.5±0.8				
	4	32.6±4.1	1.58±0.23	39.6±9.6	0.16±0.08	2.98±0.11	52.9±6.7	20.7±1.1	10.5±0.3				
	5	31±3.8	1.49±0.25	34.2±10.6	0.19±0.05	2.84±0.22	50.7±6.5	20±1.3	8.3±0.8				
	6	27.2±4.8	1.36±0.22	28.6±9.4	0.24±0.1	2.79±0.23	49±7.4	18.2±1.8	2.2±0.8				
LN	1	22.7±3.2	1.57±0.24	25.3±6.6	0.07±0.06	2.7±0.54	54.3±10.7	21.1±7.5	24.4±1.4	7.5±2.1	16.6±1.3	14.1±1.5	195±20
	2	26.9±6.6	1.43±0.31	29.6±11	0.07±0.07	2.62±0.21	53.1±10.8	19.5±3.1	14.6±2.2				
	3	27.7±8	1.39±0.36	30.6±14	0.14±0.06	2.46±0.2	52.3±10.9	19.1±4	13±0.7				
	4	31.5±4	1.48±0.28	36.2±9.3	0.16±0.08	2.15±0.23	56.6±3.8	20.6±1.4	9.6±1.2				
	5	27.6±6.5	1.36±0.31	30.1±12.1	0.19±0.07	2.03±0.17	54.3±4.5	19.6±2.4	6.6±2.5				
	6	27.1±6.2	1.46±0.19	29.4±11.1	0.2±0.07	1.92±0.18	52.8±3.8	18.1±2.5	2.9±1.7				

HN, high-nitrogen treatment; IL, internode length (cm); LA, leaf area (cm^2); LBA, leaf base angle (radian); LL, leaf length (cm); LN, low-nitrogen treatment; LNC, leaf nitrogen concentration (%); LP, leaf position from top to bottom; LSL, leaf sheath length (cm); NT, nitrogen treatment; PBN, panicle primary branch number; PL, panicle length (cm); SLW, specific leaf weight ($g\ m^{-2}$); TGN, total grain number; TN, tiller number.

a particular architectural parameter depends on the values of other architectural parameters.

Discussion

3dCAP is an integrated platform to support rice canopy photosynthesis research

The new canopy photosynthesis model 3dCAP has several new features. First, the whole architecture model includes independent models representing major rice plant organs, including leaf, panicle, stem, and sheath (Fig. 1; Supplementary Fig. S1), with each model being easily replaceable or extendable by models with even greater mechanistic detail or for other plant species. In 3dCAP, 3D architectures for all organs were modeled simultaneously, representing a major step from earlier efforts in which highly detailed 3D models of some but not all organs were developed (Ding *et al.*, 2010; Zhang *et al.*, 2017). Second, in 3dCAP, the architecture model was combined with a forward ray-tracing algorithm (Song *et al.*, 2013), a mechanical model of weight distribution, and a classical leaf photosynthetic model (Farquhar *et al.*, 1980), which together form an integrated 3D canopy photosynthesis modeling platform. The ray-tracing algorithm, the mechanical model of weight distribution, and the photosynthesis model were developed following a modular design principle, that is, they can be extended or replaced by other algorithms or models if necessary or available. Third, a workflow for the effective parameterization of 3dCAP was developed, which enables a user to easily parameterize a 3D rice canopy photosynthesis model, even if no access to complex 3D reconstruction platforms is available to the user (Fig. 2). Here we show that 3dCAP, developed and parameterized with this workflow, realistically predicted the canopy architecture and diurnal changes in canopy photosynthetic CO_2 uptake rates (Figs 4, 5; Supplementary Fig. S4). With such complete coverage of all organs following a modular design principle, full integration of the canopy architecture with internal microclimate, leaf physiology and mechanical properties, and a robust parameterization workflow, 3dCAP can be used not only independently as a tool to study canopy photosynthesis, but also as a basic module to support 3D canopy photosynthesis calculations in the current efforts of creating the 'Plants *in silico*' platform to support the global plant research community (Zhu *et al.*, 2016).

3dCAP as a tool for ideotype design

In current crop breeding programs, morphological parameters including plant height, leaf length and width, base angles and curvature of leaves at different canopy depths, panicle size, posture, and position within a canopy, tiller number, and tiller angle during the grain filling stages are used as major selection targets (Yuan, 1998; Qian *et al.*, 2016). Although a number of ideotypes have been proposed (Peng *et al.*, 1994; Yuan 1998; 2001; Chen *et al.*, 2000), many parameters in these ideotypes are defined qualitatively rather than quantitatively. This is mainly due to the lack of a robust approach to quantitatively define the optimal combinations of parameters for

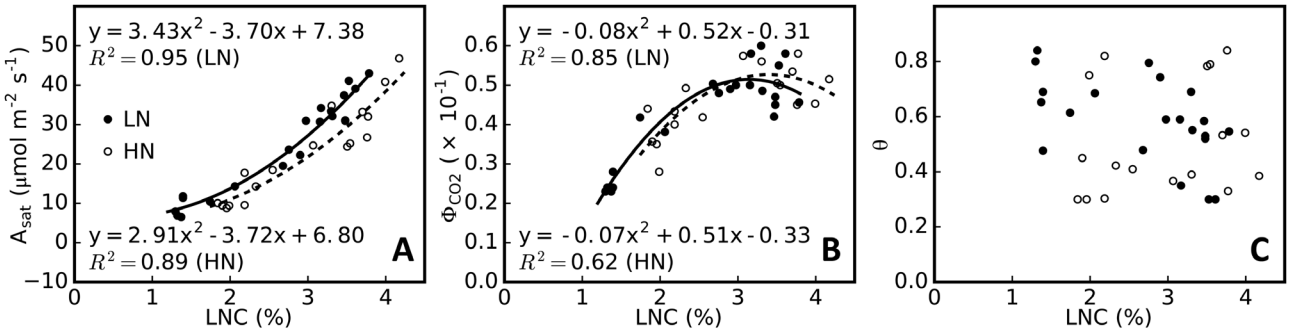

Fig. 3. Relationship between leaf nitrogen concentration (LNC) and leaf photosynthetic parameters. The correlation study was performed for high-nitrogen (HN) treatment (n=17) and low-nitrogen (LN) treatment (n=21). The leaf photosynthetic parameters used include light-saturated photosynthetic rate A_{sat} (A), maximum apparent quantum yield for CO_2 (Φ_{CO2}) (B), and curvature factor (θ) of the response of photosynthetic CO_2 uptake to incident photosynthetic photon flux density (A-PPFD) (C). LNC was calculated as LNC=(leaf nitrogen dry weight)/(leaf dry weight)×100%.

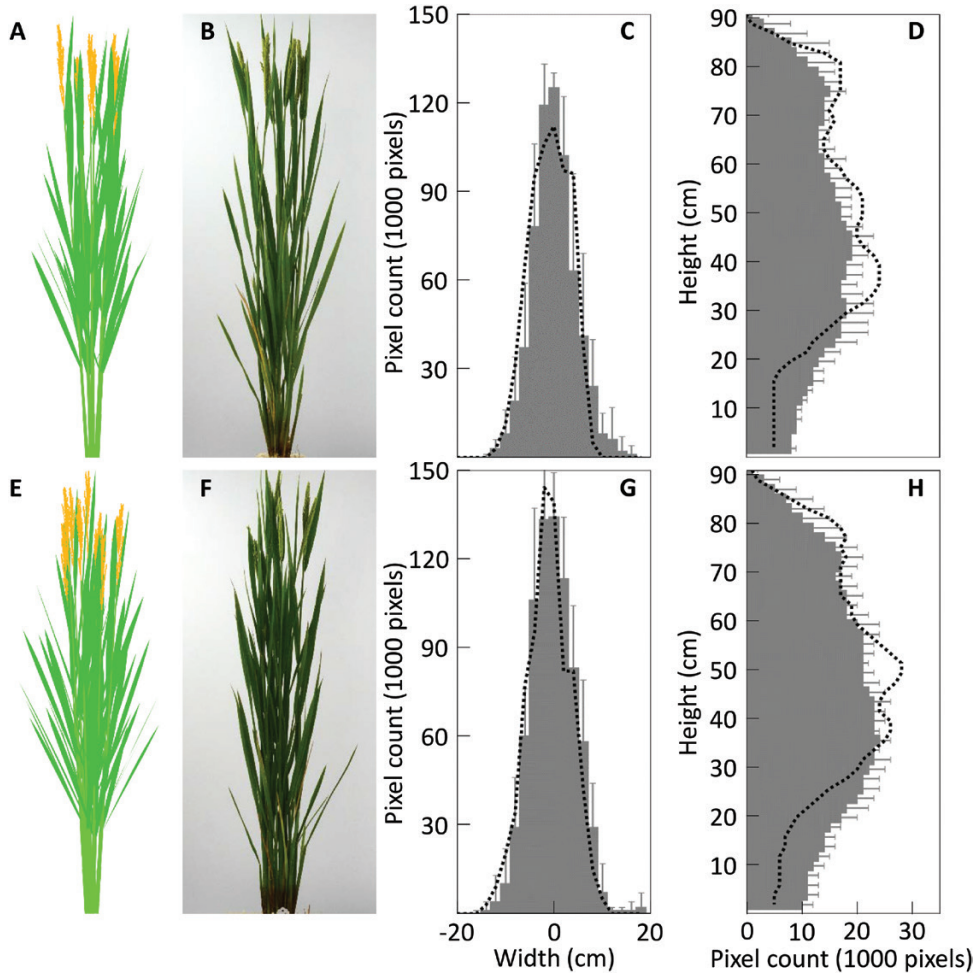

Fig. 4. Comparison of reconstructed and photographed plant architectures of rice cultivar XS134. The front view of reconstructed and photographed rice plants under low-nitrogen treatment (A, B) and high-nitrogen treatment (E, F) are shown. Counts of the number of 'plant pixels' that represent plant tissues in the images of reconstructed and photographed plants were made for plants under low-nitrogen (C, D) and high-nitrogen (G, H) treatment. The bars represent data for photographed plants (mean ±SD, n=5) and the dashed lines represent data for reconstructed plants. (This figure is available in colour at *JXB* online.)

higher canopy photosynthesis. The 3dCAP tool fills this gap by realistically representing critical features of major organs of rice, and hence enables quantitative evaluation. Here, we used the newly gained capacity provided by 3dCAP to explore potential options to improve canopy architecture for higher canopy photosynthesis in XS134, an elite rice cultivar, in the region surrounding Shanghai and Jiangsu, China. First, we found that by changing the tiller number, tiller angle, and leaf angle individually, canopy photosynthesis can potentially increase by 10–52% (Fig. 6), suggesting that there is still considerable scope to modify canopy architecture for improved canopy RUE in XS134. Second, we found a large variation

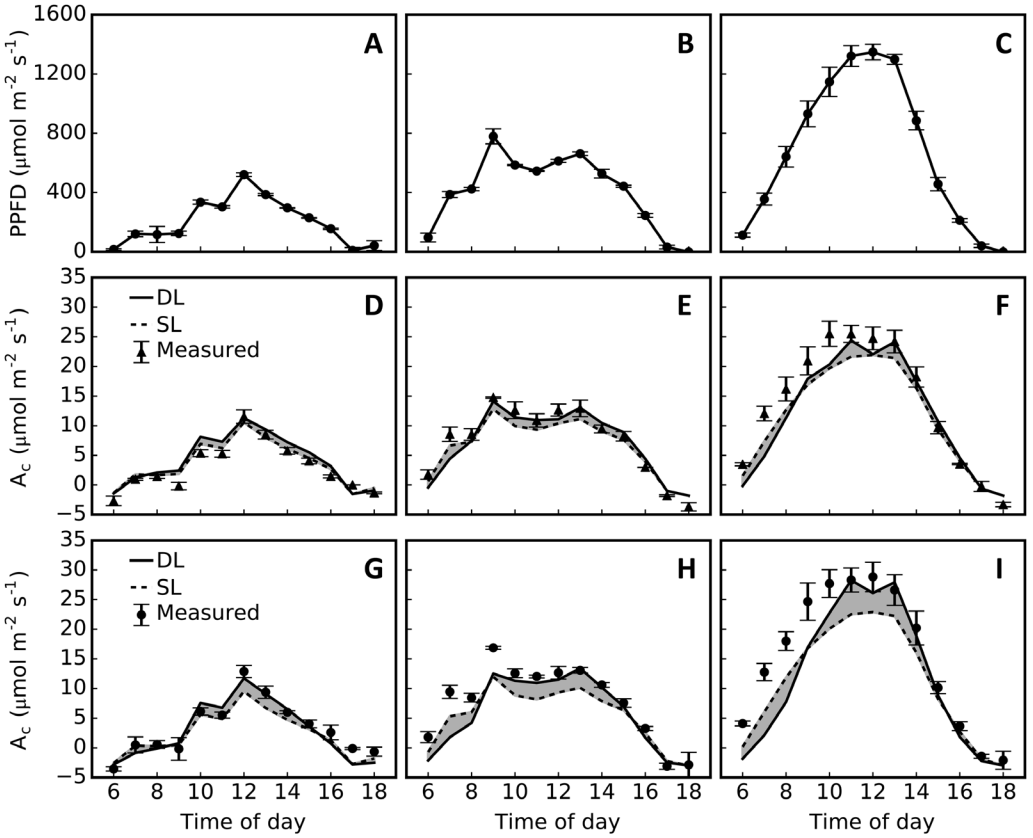

Fig. 5. Predicted and measured diurnal net canopy photosynthesis rate (A_c) on three different days. The measured hourly average photosynthetic photon flux density (PPFD) (A–C; *n*=6), A_c under low-nitrogen treatment (D–E; *n*=3) and high-nitrogen treatment (G–I; *n*=3) for rice cultivar XS134 during the daytime are shown. The simulation of diurnal A_c assumed all the incident light to be direct light only (DL) or scattered light only (SL). Diurnal light environments from three days with different weather conditions, an overcast day (12 September; A), a cloudy day (18 September; B), and a sunny day (13 September; C), were used in the simulations.

between optimal canopy architectural parameters for plants in different nitrogen treatments and under different light levels (Fig. 6). Remarkably, even for the same nitrogen treatment and light conditions, predicted elite canopy architectures can differ greatly (Supplementary Fig. S5). This, on the one hand, explains the huge variation in ideotypes proposed by different breeders (Peng *et al.*, 1994; Setter *et al.*, 1995; Yuan, 1997; Chen *et al.*, 2000). On the other hand, it indicates that the coordination of potential influencing factors, rather than one or a few parameters, determines canopy photosynthetic CO_2 uptake. Therefore, a full consideration of all features is required during the evaluation and engineering of canopy RUE in future crop breeding research, because the effect of modifying one particular parameter on canopy photosynthesis may depend heavily on the current values of other parameters.

3dCAP helps reveal features required for high canopy RUE

One of the major uses of 3dCAP is to identify features that are associated with higher canopy RUE. In this study, we used 2080 *in silico* plant architectures and evaluated their ACP under a HN condition. Specifically, we studied relationships between ACP and the three canopy architecture parameters leaf area index (calculated on the basis of leaf size and tiller number), mean leaf angle for all leaf positions, and tiller angle. We found that ACP had a non-linear relationship with leaf area index and mean leaf angle under both direct light and scattered light (Fig. 7A, B, D, E), which was consistent with experimental observations (Duncan *et al.*, 1971; Chen *et al.*, 1991). Notably, optimal canopy architecture cannot be simply determined from the empirical relationship derived from the average ACP and the average values of individual features. For example, under direct light, the optimal mean leaf angle indicated from the empirical relationship is 32°, but it was ~22.5° when ACP reached its maximum (Fig. 7B). Interestingly, ACP was not correlated with tiller angle under direct light (Fig. 7C), while high ACP can be achieved only with a small tiller angle under scattered light (Figs 6I, S, 7F).

As mentioned above, ACP can be potentially increased by 10–52% my manipulation of only a single parameter in the rice cultivar XS134 (Fig. 6; Supplementary Fig. S5). Interestingly, these manipulations potentially resulted in similar ACP with different combinations of parameter sets (Fig. 6), as shown in Supplementary Fig. S5, where two dramatically different architectures can achieve similar ACP under each combination of light condition (i.e., direct or scattered) and nitrogen treatment (i.e., HN or LN). What are the common features between these different plant architectures, especially those that can result in high ACP? We compared daily total canopy leaf-accumulated absorbed light (TLAL) and photosynthetic features of leaves at different canopy positions: that is, daily accumulated absorbed light,

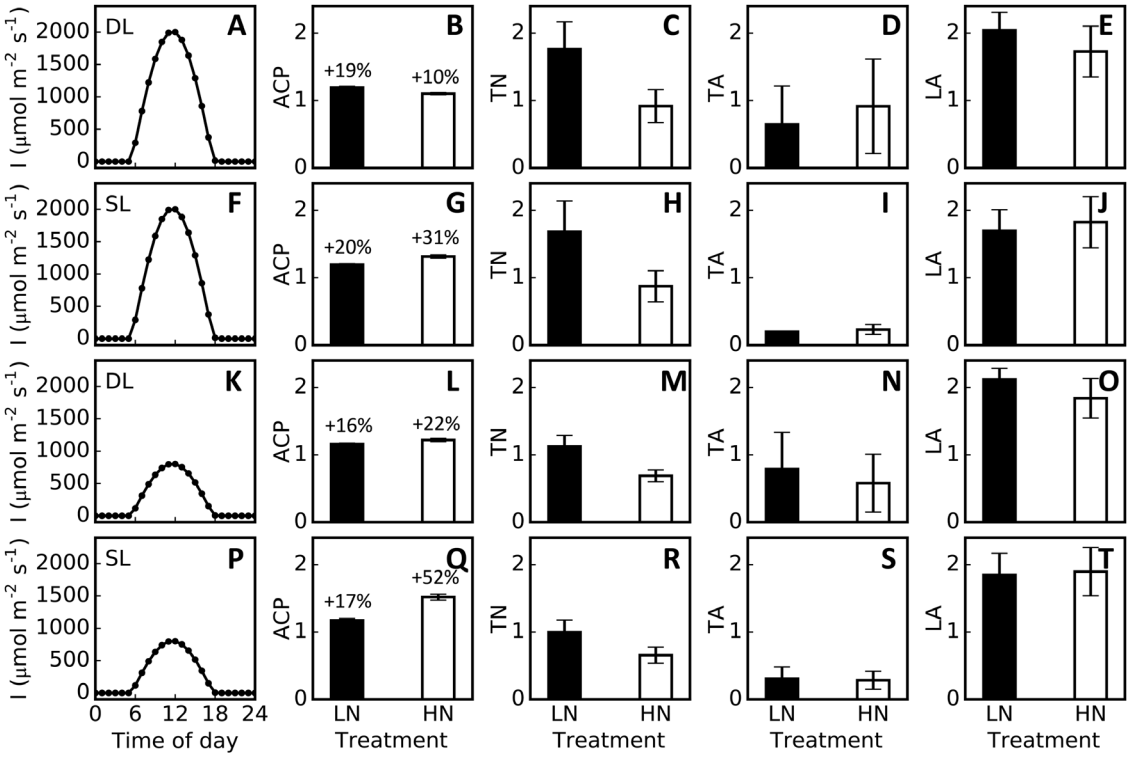

Fig. 6. Optimization of canopy architectural parameters to increase canopy photosynthesis. Optimal plant architectures for high canopy photosynthesis were identified under strong direct light (DL) only (A), strong scattered light (SL) only (F), weak DL only (K), and weak SL only (P). The parameters used to identify the optimal plant architectures are tiller number (TN) (C, H, M, R), tiller angle (TA) (D, I, N, S), and leaf angle (LA) (E, J, O, T). The top 50 plant architectures showing higher daily net canopy photosynthesis (A_c) were used in calculations of relative changes for daily net canopy photosynthetic accumulation (ACP), TN, TA, and LA. The numbers above the bars in panels B, G, L, and Q represent relative change from the respective values for default plants.

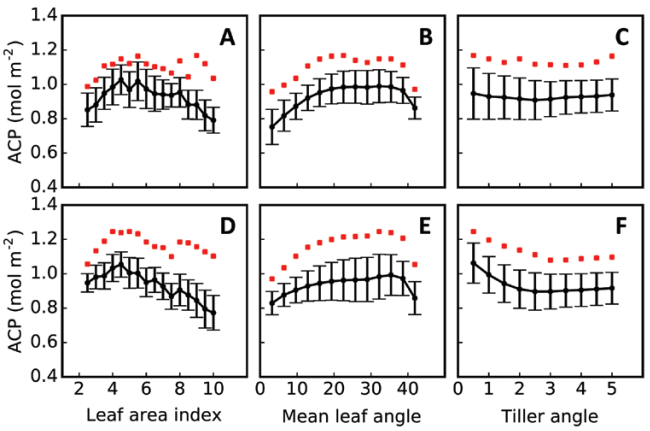

Fig. 7. Relationships between simulated daily net canopy photosynthetic accumulation (ACP) and plant architectural parameters under two light conditions, strong direct light only (A–C; see Fig. 6A) and strong scattered light only (D–F; see Fig. 6F), simulated for rice cultivar XS134 under high-nitrogen treatment. The black dots with error bars show the predicted variations of ACP for 2280 plant architectures with different combinations of tiller number, tiller angle, and leaf angle. The red squares denote optimal ACP values. The mean leaf angle is the average value for all leaves on a plant. (This figure is available in colour at *JXB* online.)

daily photosynthetic CO_2 uptake and LNC. First, we found that elite canopy architectures (the 'Top 50' in Fig. 8A, D) had more TLAL than the default canopy ('CK' in Fig. 8A, D), especially under the scattered light condition (Fig. 8D). Second, the increase in ACP for elite canopy architectures compared with the default canopy was derived mainly from the lower leaves in the canopy (Fig. 8C, F) rather than the flag leaves. For the default canopy, daily average light absorption for the lower leaves was low (Fig. 8B, E), especially under the scattered light condition (Fig. 8E). Notably, canopy architectures with high TLAL may not necessarily achieve high canopy RUE. An extreme example is given in Fig. 9, in which a canopy with very high TLAL had lower ACP as a result of much lower light partitioning to the flag leaves, which have a high nitrogen concentration, and higher light partitioning to the lower leaves, which have lower leaf nitrogen concentration—that is, in this canopy there is a lack of coordination between light distribution and nitrogen distribution. These results suggested that both daily total canopy leaf light interception and coordination between nitrogen concentration and light interception for each leaf (Fig. 8C, F) are critical to canopy RUE. These two key features might underlie the mechanism of high canopy RUE by optimizing plant architecture.

In addition, on average, panicles were predicted to absorb 30% of canopy total absorbed light under direct light and 41% under scattered light, which represents a substantial proportion of incident light energy. This is significant because there are large variations of panicle position among current elite rice lines. For example, while the XS134 used in this study is a typical *japonica* rice cultivar, most of the current *indica* rice cultivars have drooping panicles at the middle of a canopy (Setter *et al.*, 1995; Yuan, 2017). Therefore, the new model can

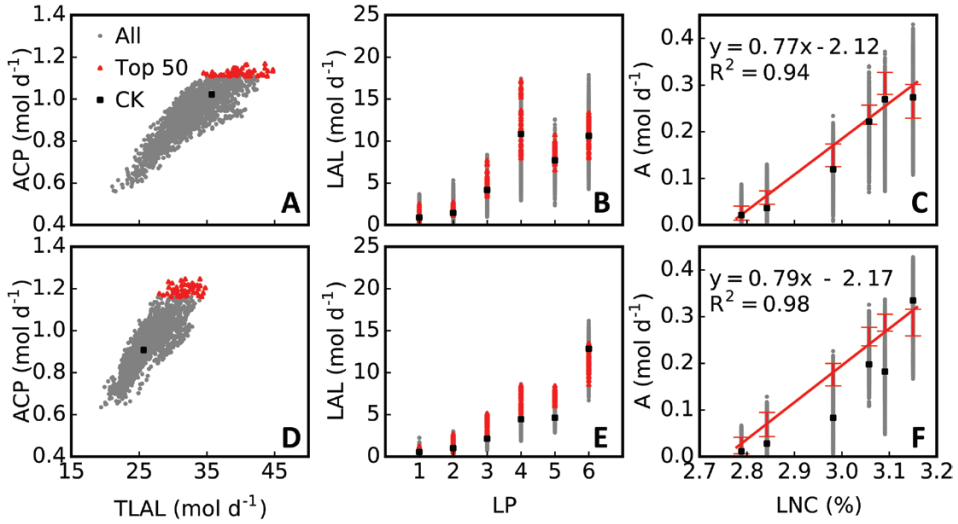

Fig. 8. Relationships between simulated photosynthesis, light interception, and leaf nitrogen concentration. Two light conditions, strong direct light (A–C; see Fig. 6A) and strong scattered light (D–F; see Fig. 6F), were used for rice cultivar XS134 under high-nitrogen treatment. The relationships between daily total canopy leaf-accumulated absorbed light (TLAL) and daily net canopy photosynthetic CO_2 uptake (ACP; A, D), between leaf position (LP; counted from bottom to top on a plant) and daily total light absorption by a leaf (LAL; B, E), and between leaf nitrogen concentration (LNC) and leaf daily total photosynthetic CO_2 uptake (*A*; C, F) are illustrated for 2280 plant architectures (All), elite plant architectures (Top 50), and the default plant architecture (CK). ACP, TLAL, LAL, and *A* were calculated for 1 m^2 ground area.

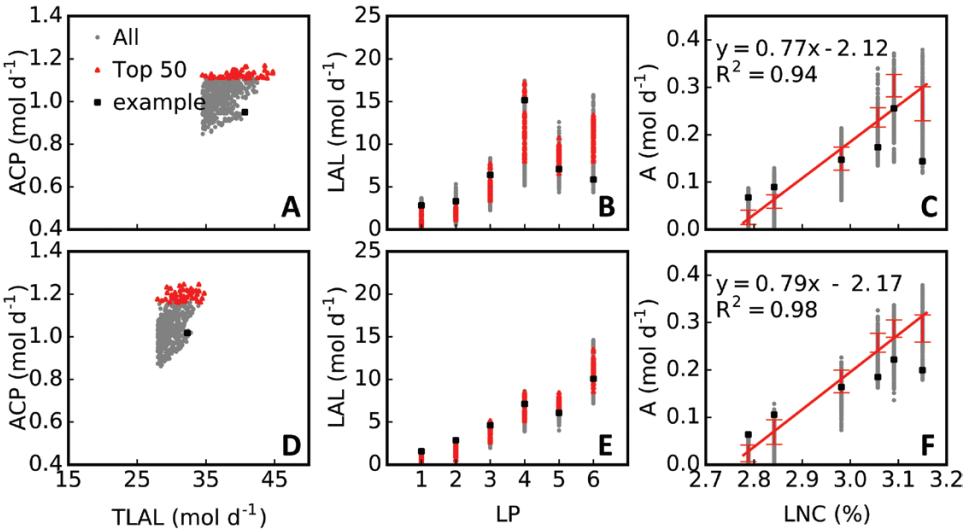

Fig. 9. Relationships between simulated photosynthesis, light interception, and leaf nitrogen concentration. Two light conditions, strong direct light (A–C; see Fig. 6A) and strong scattered light (D–F; see Fig. 6F), were used for rice cultivar XS134 under high-nitrogen treatment. The relationships between daily total canopy leaf-accumulated absorbed light (TLAL) and daily net canopy photosynthetic CO_2 uptake (ACP; A, D), between leaf position (LP; counted from bottom to top on a plant) and daily total light absorption by a leaf (LAL; B, E), and between leaf nitrogen concentration (LNC) and leaf daily total photosynthetic CO_2 uptake (*A*; C, F) are illustrated for simulated plant architectures with high TLAL (All), elite plant architectures with high ACP (Top 50), and a plant architecture with high TLAL but low ACP (example). ACP, TLAL, LAL, and *A* were all calculated for 1 m^2 ground area.

be used as a tool to study the impacts of panicle position and shape on canopy photosynthesis.

Supplementary data

Supplementary data are available at *JXB* online.

Fig. S1. Reconstruction of the 2D and 3D architecture of a rice leaf.

Fig. S2. The workflow of 3dCAP reconstruction and canopy photosynthesis calculation.

Fig. S3. Different views of reconstructed rice plants.

Fig S4. Predicted and measured net canopy photosynthesis rates under different incident light intensities at different times of day.

Fig. S5. Difference among predicted optimal plant architectures for optimal daily total canopy photosynthetic CO_2 uptake.

Acknowledgements

This research was financially supported by the CAS strategic leading project 'modular designer crop breeding' (grant no. XDA08020301), a CAS international collaboration grant (grant no. GJHZ1501), and

the National High Technology Development Program (grant no. 2014AA101601).

Data availability

This model and the corresponding parameterization protocol and detailed user manuals are freely accessible on GitHub (https://rootchang.github.io/3dCAP/). The source code is available for research and teaching purposes on request from the authors. The model can be freely used for academic purposes. For commercial purposes, a special license is required.

References

Amthor JS. 1994. Scaling CO_2-photosynthesis relationships from the leaf to the canopy. Photosynthesis Research **39,** 321–350.

Chang TG, Xin CP, Qu MN, Zhao HL, Song QF, Zhu XG. 2017. Evaluation of protocols for measuring leaf photosynthetic properties of field-grown rice. Rice Science **24,** 1–9.

Chang TG, Zhu XG, Raines C. 2017. Source–sink interaction: a century old concept under the light of modern molecular systems biology. Journal of Experimental Botany **68,** 4417–4431.

Chen W, Xu Z, Zhang W, Zhang L, Yang S. 2000. Creation of new plant type and breeding rice for super high yield. Acta Agronomica Sinica **27,** 665–672.

Chen W, Xu Z, Zhong L. 1991. Studies on canopy properties and its relation to dry matter production in japonica rice varieties with different plant types. Chinese Journal of Rice Science **5,** 67–71.

Cieslak M, Lemieux C, Hanan J, Prusinkiewicz P. 2008. Quasi-Monte Carlo simulation of the light environment of plants. Functional Plant Biology **35,** 201–204.

De Pury D, Farquhar G. 1997. Simple scaling of photosynthesis from leaves to canopies without the errors of big-leaf models. Plant, Cell & Environment **20,** 537–557.

de Wit CT. 1965. Photosynthesis of leaf canopies. Agricultural Research Report No. 663. Wageningen: PUDOC.

Ding W, Liu C, Zhang Y, Zhu D, Zhang Q, Gu H. 2010. Visually modeling spatial shape of rice panicle based on calculation of bending deformation. Chinese Journal of Rice Science **24,** 309–314.

Duncan WG. 1971. Leaf angles, leaf area, and canopy photosynthesis. Crop Science **11,** 482–485.

Farquhar G, von Caemmerer SV, Berry J. 1980. A biochemical model of photosynthetic CO_2 assimilation in leaves of C_3 species. Planta **149,** 78–90.

Feret JB, François C, Asner GP, Gitelson AA, Martin RE, Bidel LPR, Ustin SL, Maire GL, Jacquemoud S. 2008. PROSPECT-4 and 5: advances in the leaf optical properties model separating photosynthetic pigments. Remote Sensing of Environment **112,** 3030–3043.

Fournier C, Andrieu B. 1998. A 3D architectural and process-based model of maize development. Annals of Botany **81,** 233–250.

Fournier C, Andrieu B. 1999. ADEL-maize: an L-system based model for the integration of growth processes from the organ to the canopy. Application to regulation of morphogenesis by light availability. Agronomie **19,** 313–327.

Fritsch FN, Carlson RE. 1980. Monotone piecewise cubic interpolation. Siam Journal on Numerical Analysis **17,** 238–246.

Gu J, Yin X, Stomph T-J, Struik PC. 2014. Can exploiting natural genetic variation in leaf photosynthesis contribute to increasing rice productivity? A simulation analysis. Plant, Cell & Environment **37,** 22–34.

Henke M, Kurth W, Buck-Sorlin GH. 2016. FSPM-P: towards a general functional-structural plant model for robust and comprehensive model development. Frontiers of Computer Science **10,** 1103–1117.

Ishihara K, Saitoh K. 1987. Diurnal courses of photosynthesis, transpiration, and diffusive conductance in the single-leaf of the rice plants grown in the paddy field under submerged condition. Japanese Journal of Crop Science **56,** 8–17.

Li T, Hasegawa T, Yin XY, *et al*. 2015. Uncertainties in predicting rice yield by current crop models under a wide range of climatic conditions. Global Change Biology **21,** 1328–1341.

Lloyd J, Grace J, Miranda AC, Meir P, Wong SC, Miranda HS, Wright IR, Gash JHC, Mcintyre J. 1995. A simple calibrated model of Amazon rainforest productivity based on leaf biochemical properties. Plant Cell & Environment **18,** 1129–1145.

Maiorano A, Martre P, Asseng S, *et al*. 2017. Crop model improvement reduces the uncertainty of the response to temperature of multi-model ensembles. Field Crops Research **202,** 5–20.

Markwell J, Osterman J, Mitchell J. 1995. Calibration of the Minolta SPAD-502 leaf chlorophyll meter. Photosynthesis Research **46,** 467–472.

Mech R. 1997. Modeling and simulation of the interaction of plants with the environment using L-systems and their extensions. Calgary: University of Calgary.

Peng S. 2000. Single-leaf and canopy photosynthesis of rice. Studies in Plant Science **7,** 213–228.

Peng S, García FV, Laza RC, Cassman KG. 1993. Adjustment for specific leaf weight improves chlorophyll meter's estimate of rice leaf nitrogen concentration. Agronomy Journal **85,** 987–990.

Peng S, Khush G, Cassman K. 1994. Evolution of the new plant ideotype for increased yield potential. In: Breaking the yield barrier. Proceedings of a workshop on rice yield potential in favourable environments. Los Baños: International Rice Research Institute, 5–20.

Qian Q, Guo LB, Smith SM, Li JY. 2016. Breeding high-yield superior quality hybrid super rice by rational design. National Science Review **3,** 283–294.

Setter T, Conocono E, Egdane J, Kropff M. 1995. Possibility of increasing yield potential of rice by reducing panicle height in the canopy. I. Effects of panicles on light interception and canopy photosynthesis. Functional Plant Biology **22,** 441–451.

Song Q, Chu C, Parry MA, Zhu XG. 2016a. Genetics-based dynamic systems model of canopy photosynthesis: the key to improve light and resource use efficiencies for crops. Food & Energy Security **5,** 18–25.

Song Q, Xiao H, Xiao X, Zhu X-G. 2016b. A new canopy photosynthesis and transpiration measurement system (CAPTS) for canopy gas exchange research. Agricultural and Forest Meteorology **217,** 101–107.

Song QF, Zhang GL, Zhu XG. 2013. Optimal crop canopy architecture to maximise canopy photosynthetic CO_2 uptake under elevated CO_2 - a theoretical study using a mechanistic model of canopy photosynthesis. Functional Plant Biology **40,** 109–124.

Tucker CJ, Garratt MW. 1977. Leaf optical system modeled as a stochastic process. Applied Optics **16,** 635–642.

Wang Y, Song QF, Jaiswal D, de Souza AP, Long SP, Zhu XG. 2017. Development of a three-dimensional ray-tracing model of sugarcane canopy photosynthesis and its application in assessing impacts of varied row spacing. Bioenergy Research **10,** 626–634.

Watanabe T, Hanan JS, Room PM, Hasegawa T, Nakagawa H, Takahashi W. 2005. Rice morphogenesis and plant architecture: measurement, specification and the reconstruction of structural development by 3D architectural modelling. Annals of Botany **95,** 1131–1143.

Xu L, Henke M, Zhu J, Kurth W, Buck-Sorlin G. 2011. A functional-structural model of rice linking quantitative genetic information with morphological development and physiological processes. Annals of Botany **107,** 817–828.

Yuan L. 1997. Hybrid rice breeding for super high yield. Hybrid Rice **12,** 1–3. (in Chinese)

Yuan L. 2001. Breeding of super hybrid rice. International Rice Research Conference. Los Baños: International Rice Research Institute, 31 March–3 April 2000.

Yuan L. 2017. Progress in super-hybrid rice breeding. The Crop Journal **5,** 100–102.

Zhang Y-H, Tang L, Liu X-J, Liu L-L, Cao W-X, Zhu Y. 2017. Modeling curve dynamics and spatial geometry characteristics of rice leaves. Journal of Integrative Agriculture **16,** 2177–2190.

Zheng B, Shi L, Ma Y, Deng Q, Li B, Yan G. 2008. Comparison of architecture among different cultivars of hybrid rice using a spatial light model based on 3-D digitising. Functional Plant Biology **9,** 900–910.

Zhu XG, Lynch JP, LeBauer DS, Millar AJ, Stitt M, Long SP. 2016. Plants *in silico*: why, why now and what?—an integrative platform for plant systems biology research. Plant, Cell & Environment **39,** 1049–1057.